Modelling of the heat-affected and thermomechanically affected zones in a Ti-6Al-4V inertia friction weld

Turner, Richard; Perumal, Bama; Lu, Yu; Ward, Mark; Basoalto, Hector; Brooks, Jeffery

DOI:
10.1007/s11663-018-1489-z
10.1007/s11663-018-1489-z

Modelling of the Heat-Affected and Thermo-Mechanically-Affected Zones in a Ti-6Al-4V Inertia Friction Weld

R.P. Turner*, B. Perumal, Y. Lu, R.M. Ward, H.C. Basoalto and J.W. Brooks

PRISM[2] Research Group, School of Metallurgy & Materials, University of Birmingham, Birmingham, B15 2TT, UK

*Corresponding author: r.p.turner@bham.ac.uk

Abstract

Inertia friction welding has been used across the aerospace, automotive and power-generation industries for the fabrication of complex axi-symmetric components for over forty years. The process sees one axi-symmetric piece held stationary and another piece brought in to contact set to rotate about its axis of symmetry by a flywheel with the system under an applied load across the joint. Plasticization at the joint interface through the frictional heating sees the two pieces bond together. The titanium alloy Ti-6Al-4V has been widely studied for inertia welding applications. A successful selection of processing parameters (flywheel energy and mass, applied load) allows an inertia welding process which produces a very high-integrity weld, with a minimal heat-affected zone (HAZ) and thermo-mechanically affected zone (TMAZ), formed as a narrow band at the interface and extending away in to the material. The width of this narrow band of heated material is dependent upon the process parameters used. A series of experimental inertia friction welds were performed using Ti-6Al-4V, and a finite element modelling framework was developed using the FE code Deform in order to predict the widths of the HAZ and TMAZ at the weld interface. The experimentally observed HAZ boundaries were correlated with the thermal fields from the FE model, whilst TMAZ boundaries were correlated with the Von Mises plastic strain fields.

Introduction

Friction welding techniques are becoming a more wide-spread and popular processing route for fabrication of complex components across a number of industries, notably aerospace [1], automotive [2], transportation [3] and power-generation. This is largely due to the concomitant benefits of microstructural refinement and controlled residual stresses [4] achieved due to the thermal, mechanical and microstructural evolution at the interface region of the two faying surfaces during a friction weld, when compared with a more traditional fusion welding technique. One of the key features of a typical friction welded processing route is that the interface material is generally not raised above the solidus temperature. Thus, the process is often referred to as a solid-state joining method [5].

Although the issue of material melting in inertia friction welding (or just inertia welding) is a controversial one, it is widely understood that across some friction welding applications using certain materials, it is possible to observe some small-scale material melting in localized regions and hot-spots [5]. The prevalence for this highly localized melting is exacerbated by a poor selection of process parameters, leading to an overly energetic friction welding process for the material selected. Additionally, for some materials used in friction welding processes, interfacial melting can be observed [6] for even a successful welding parameter set. However, one of the major reasons for friction welding being used as a processing route is due to the fact that the interface material is not heated significantly above the solidus, thus avoiding the production of bulk liquid phase within the sample, and thus reducing problems associated with liquation or solidification cracking.

Controlling the microstructural evolution of the interface material [7-8] for a range of 'friction-weldable' materials is of considerable importance to component manufacturers, as it is precisely the formed microstructure that dominates the properties of the joint. A method to target a specific microstructural evolution at specific regions of the material, such as the interface, allows for location-specific-property design, which can aid the component significantly in terms of life-prediction and strength. Additionally, the significant variation in microstructure from parent material to the interface material will modify the residual stress across the component weld interface [8]. Thus an understanding of how the interface region microstructure has changed, away from its original parent condition, is advantageous.

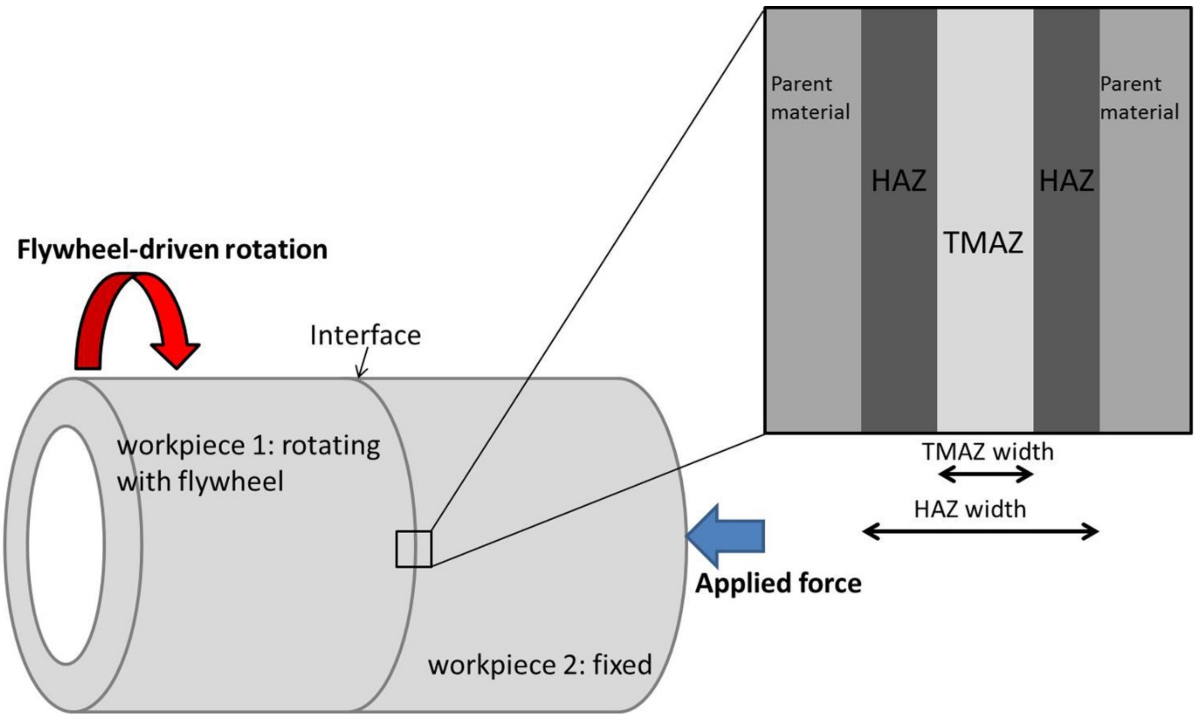

Figure 1: Schematic of an inertia weld on a hollow cylinder, showing a macro-scale representation of the banding of parent, HAZ and TMAZ material.

The presence of the heat affected zone (HAZ) and the thermo-mechanically affected zone (TMAZ) across the weld interface within an inertia friction welded joint has been widely considered by researchers previously. Nessler [9] evidenced that HAZ regions for a titanium alloy inertia weld were narrow, of typically 3mm or smaller. Similarly Attallah [10] reviewed Ti-6Al-4V HAZ regions from an inertia weld, and demonstrated further evidence from the literature [11] of Widmanstatten α (or transformed β grains) at the interface, through the combination of heating rates and strains experienced.

Baeslak [12] studied the inertia welding of a less common titanium alloy, and classified the weld interface region in to an inner heat and deformation zone (Inner-HDZ), 25μm wide with dynamically recrystallized fine β grains, and an outer heat and deformation zone (Outer-HDZ), 500μm wide containing transformed β with α clusters. In addition to these, a different titanium alloy, Ti-6Al-2Sn-4-Zr-2Mo was evidenced to contain a refined lamellar α structure present in the HAZ [13]. Whilst Pardhi [14] noted that the HAZ for a titanium alloy Ti-6Al-2Sn-4Zr-6Mo contained needle like martensitic α in between a fine equiaxed β grain structure. Finally, Yates [15] commented on the microstructural properties of the HAZ in a titanium inertia weld, such that the weld region is actually improved in terms of its susceptibility for tensile failure or low-cycle fatigue problems, compared to the parent material.

A typical inertia welded sample is understood to be subjected to severe thermal and mechanical loadings during processing. The material, if viewed as a cross section perpendicular to the mating interface, can be split in to a number of distinct regions based upon the local microstructure [5,7,16]. In these titanium alloy welds, parent material is referred to as material which has never exceeded the β-transus temperature, and has as such remained in its original microstructural condition. Heat-affected zone (HAZ) material is material which has exceeded the β-transus temperature for sufficiently long enough for the material to undergo the allotropic transformation. Given the rapid nature of a friction weld process, further understanding of time required above the β-transus temperature for the allotropic transformation to fully occur is required. The HAZ region is commonly thought of as being made up of several sub-regions [5], namely the un-deformed heated region, the fully plasticized region and the partially plasticized / partly deformed region [5]. The thermo-mechanically-affected zone (TMAZ), for the purpose of this work, is considered to be the combined "fully-plasticized" and "partially plasticized" regions. This is the narrow band of material, in-between the regions of un-deformed HAZ, which has experienced elevated temperatures and the severe shear deformation caused by the relative rotating motion of one side of the weld geometry in relation to the other side – see Figure 1.

Numerical modelling of the friction welding processes for titanium alloys, as well as other aerospace materials, has largely focused upon accurate predictions of more macro-scale outputs including upsetting rate, full specimen thermal profiles from room temperature up to the peak temperature, and the formation of flash. Whilst these are important macro-scale outputs, they perhaps neglect the finer intricacies of correctly predicting features such as HAZ zone, and TMAZ zone. As such, the intention of this modelling framework is to interrogate a macro-scale modelling approach developed by the authors previously [15] to assess how accurately it can predict HAZ and TMAZ zone widths, through simplistic FE thermal and mechanical fields alone - thus by-passing the need for computationally expensive metallurgical user-subroutines - to understand whether this approach is feasible and can reasonably predict HAZ and TMAZ width behavior.

Thus, this work will characterize a range of IFW samples in order to quantify the relationship between the processing parameters and the size of the HAZ and TMAZ. In addition, detailed microstructural characterization close to the HAZ and parent material interface has specifically considered the impact that rapid heating and cooling rates had upon the transformation of the α (hcp) phase for material that may have only remained above the β-transus temperature for a very short period of time.

Experimental Procedure

Inertia weld experiments were performed at the Manufacturing Technology Centre (MTC) using a 125 tonne state-of-the-art MTI inertia friction welding machine [17], using hollow cylindrical coupons of Ti-6Al-4V measuring 86mm in length, 80mm outer diameter and 40mm inner diameter. A series of welds were performed using process parameters as according to Table 1. Once the welding trials were completed, samples of material across the weld interface were sectioned from the cylinders, and metallographic analysis was performed according to the standard procedures [18] and etched with 0.5% Hydrofluoric acid (HF). Further, these samples were characterized by using Light Optical Microscopy (LOM) with a ZEISS Axioskop2 MAT microscope facility available at University of Birmingham. Additionally the metallographic samples were analyzed using a JEOL 7000F Scanning Electron microscope (SEM), part of the SEM facilities at the University of Birmingham, for the higher magnification microstructure analysis. Lastly, micro-indentation hardness testing using a Struers Emco-test DuraScan hardness testing machine was performed, to accurately measure the HAZ region. The indenting tool used had a head diameter of approximately 25 μm. Given that spacing in between successive measurements should be approximately double the indent, thus accuracy in HAZ width measurements are likely to be of the order of +/- 100 μm.

In order to better understand the microstructural evolution of Inertia welded Ti-6Al-4V interface, the influence of forging pressure and the influence of initial rotation speed on the interface microstructure of the Ti-6Al-4V cylinders were studied. The typical as-received microstructure of the base / parent material was captured. As shown in Figure 2, typically a Ti-6Al-4V alloy in its as-received condition before any Inertia weld processing has a microstructure with elongated primary alpha (α) phase distributed in the matrix of transformed beta (β) phase.

Some measurement terminology must be established now that the terms of “Heat-affected zone” and “thermo-mechanically affected zone” for these Ti-6Al-4V inertia welds are to be quantified as widths. The bandings of material left after an inertia weld sees the thermo-mechanically affected zone sandwiched between two bands of heat-affected zone, which is in turn sandwiched between the parent material. Thus, the thermo-mechanically affected zone width is characterized as the width of the band of material undergoing heating and mechanical shearing – namely the width of the fully and partially plasticized regions [5]. The heat-affected zone width is to be defined as the full width of the material from HAZ/parent interface on one side of the weld to HAZ/parent interface on the other side which has seen the solid state transformation occur – ie: the sum of the fully and partially plasticized and the un-deformed heated affected regions.

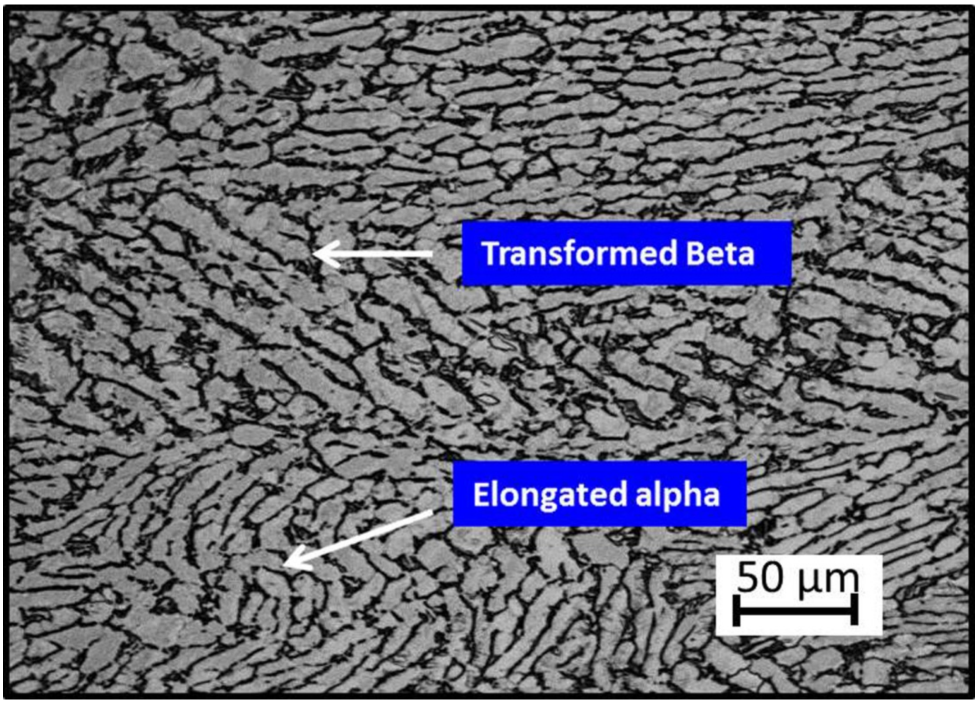

Figure 2: Elongated α grain in a transformed β matrix at x50 magnification

Table 1: Process parameters used in IFW FE modelling and experimental trials.

Weld No.	Inertia value (kgm^2)	Initial rotation speed (rad/s)	Pressure (MPa)	Total Energy $½I\omega^2$ (kJ)	Resulting Experimental Upset (mm)
1	18.6	185	100	637	14.1
2	18.6	185	80	637	13.1
3	18.6	115	40	246	2.3
4	18.6	105	40	205	1.6
5	18.6	96	40	171	1.1

Finite Element Methodology

Finite element (FE) modelling of the inertia welding process has been well-established within the literature [16, 19-22] as a successful tool for process prediction. A typical modelling strategy has been to consider the process occurring between two distinct two-dimensional objects representing the wall cross-section, with a relative rotational motion between the two parts (and an associated frictional condition between the two) throughout the duration of the process. This assumption is clearly a simplification of the real-world physical phenomena at the interface, as it is known that at some point during the process the interface must cease to act as a distinct boundary between two separate objects, and become a highly deforming region of a single object. However the above assumption has been demonstrated to produce sensible results across a number of different materials, with modelling activities performed by a selection of papers [16, 19-24].

A finite element modelling approach was constructed by the authors using the FE software DEFORM v11.1, as presented previously in the literature [22-23]. The model was defined with careful consideration of other inertia friction weld FE modelling work [19-21, 24]. A material file to represent the thermal and mechanical behavior of the titanium alloy Ti-6Al-4V was constructed, consisting of temperature dependent tabular data sets for thermal conductivity, specific heat capacity, density, Young's Modulus, Poisson ratio and thermal expansion, with data available from room temperature up to 2000 °C. Additionally, the material data set for this titanium alloy included tabulated flow stress curves ranging from room temperature to 1600°C and strain rates from 10^{-3} s^{-1} up to 10^{3} s^{-1} was specified, based on data from the thermo-mechanical materials properties database JMatPro software [25]. This would allow the thermo-physical and thermo-mechanical response of the workpiece within the model as it undergoes the relevant thermal and mechanical fields to respond as accurately as possible to represent the titanium alloy of interest.

The generation of frictional heating at the interface between the two distinct workpieces was incorporated in to the FE model by the use of boundary conditions. Boundary conditions applied related the FE model to both the thermal and mechanical restraints of the real process. Thermally, the surrounding environment was set to room temperature, and a convective heat transfer coefficient of 20 $Wm^{-2}K^{-1}$ employed. Radiative losses were assumed to be negligible, and thus ignored. Although this is clearly a simplification given the glowing of the titanium alloy when heated, this happens for such a short period of time that is it believed to be appropriate to be neglected.

Mechanically, the upper and lower workpieces were fixed with a fully sticking condition against their respective forging and flywheel tooling components, such that one piece was held stationary and the other forced to rotate with the same angular velocity as the flywheel, as per the experiment. The relative rotational speed experienced at the workpiece interface was then simulated using a shear friction condition, with a value of f dependent upon temperature, as specified in Equation 1.

$$f = aln(T) - b \qquad \text{for } 100°C < T < 1400\ °C \text{ ....(Eq. 1)}$$

Where a and b are material dependent parameters to be determined. Further details of the frictional condition, and the finite element model in general, are given in [15].

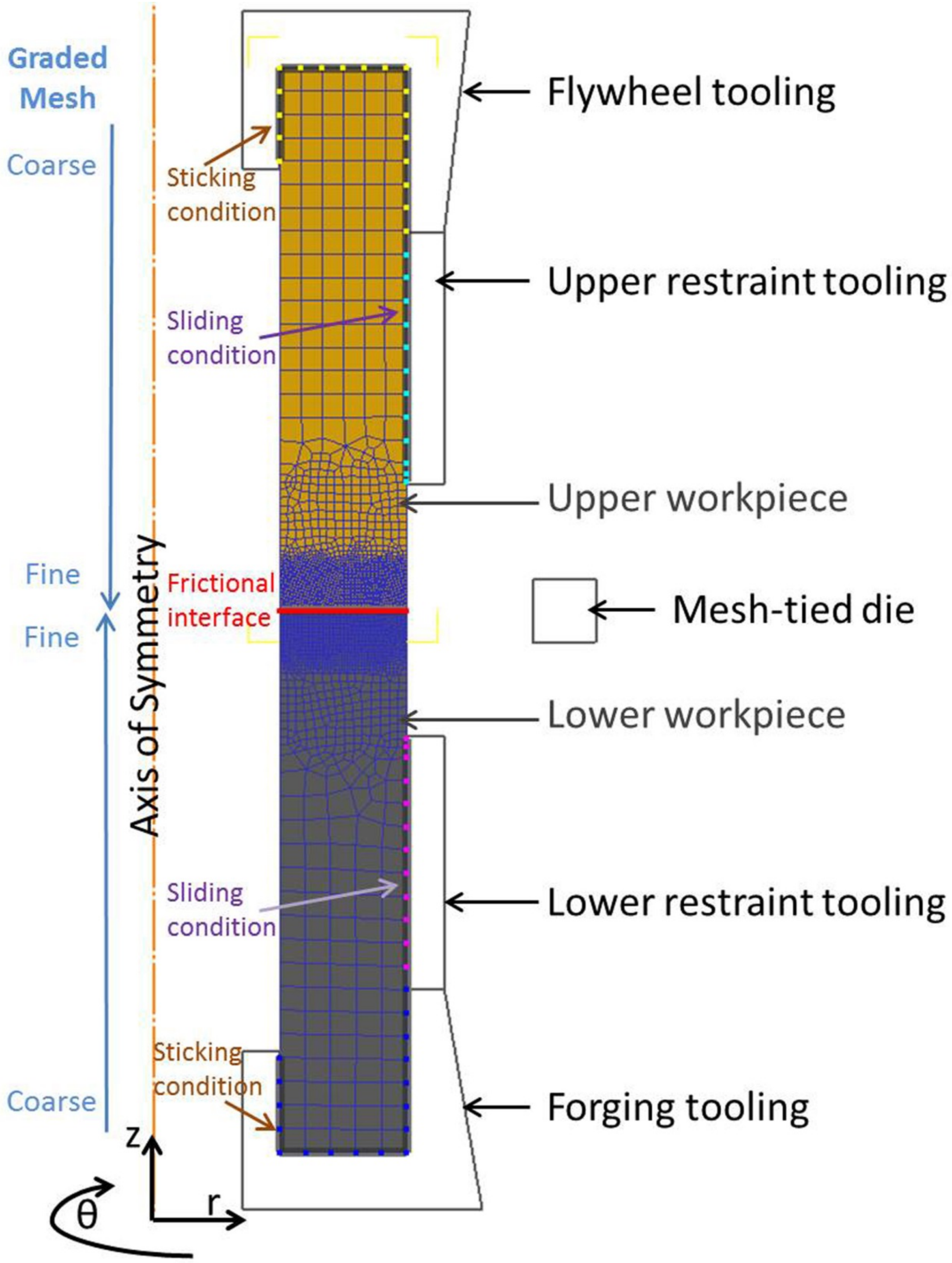

Figure 3: An example of the FE modelling set-up for the IFW modelling in Deform v11.0.

The model assumes a constant applied load throughout the process, and within the input deck the user specifies i) this applied load, ii) the inertia of the flywheel used, and iii) the total energy available to the process, as the three key process parameters specified to define the weld process. Finally, an air cooling period of over 500 seconds was applied to allow the workpieces to return to ambient temperatures.

A graded mesh (with elements measuring 0.2mm at the weld interface) was used to capture detailed thermal and mechanical gradients at the interface – see Figure 3. This was established with target windows drawn at specific locations to force mesh refinement. The model simulated the real physical boundary conditions where the two workpieces were in contact with tooling and grips.

The software was required to perform re-meshing for when the distortions to the elements, caused by the shearing and flash formation, became so severe that the calculation was no longer stable [22]. The Deform software [26] has an excellent automatic re-meshing tool, such that this can largely be monitored and re-meshed by the FE software alone, with little user input once the model is set correctly. The use of a dummy mesh-tied die allows the refined mesh windows to move at the correct velocity (half the axial upset rate, given that axial upset is even above and below the interface), and the software triggers a re-meshing step within the refined mesh window once a mesh interference depth (element impingement) reaches 0.1 mm, or up to a maximum time of 0.1 s after the onset of axial upset and deformation.

The model was created such that as a first-order approximation, i) the thermal cycles alone can be interrogated to determine the material that will be considered to have undergone the solid-state phase transformation and as such form the HAZ, and ii) the plastic strain field alone can be interrogated to give a reasonable estimate of the fully and partially plasticized material [5] of the TMAZ. The definition of the material within the model which is classified as HAZ material is anything that has experienced a thermal cycle of greater than 1256 K (983 °C). Note that no minimum time held at temperature was required, thus this may provide some uncertainty in to the predictions. The definition of the material in the model which is classified as TMAZ is anything which, additionally to exceeding 1256 K (983 °C) has also experienced a plastic strain of 0.05 or greater.

Results and Discussion

The finite element modelling thermal and mechanical outputs were interrogated to determine the predicted widths of the band of material that was; i) understood to exceed the β-transus temperature, and which was ii) predicted to experience a significant plastic strain. These fields were calculated by plotting the fields of temperature and von Mises plastic strain perpendicular to the weld line. For a fair comparison, the profile for each plastic strain field and thermal field from FE model, and the corresponding weld section analysis, was taken from the center line of the cylinder wall-thickness, when the cross-section of the wall was analyzed. The FE predictions were critically compared to experimentally measured optical microscopy results (see Figure 4) to assess the FE modelling accuracy.

As a further method of modelling validation, the volumetric shape of the flash predicted by the FE model can be compared to the real flash formation. This validation exercise would provide further evidence that the finite element model, although whilst making certain stated assumptions and simplifications to the true process, is still capable of capturing the fundamental materials and thermo-mechanical behavior. The resulting flash formation for Weld 1 is presented in Figure 5. It is demonstrated that the finite element modelling framework, with the associated boundary conditions, frictional condition, material definition and modelling parameters (time-stepping, mesh density) used can predict with some accuracy the formation of the flash material, in terms of its shape and appearance.

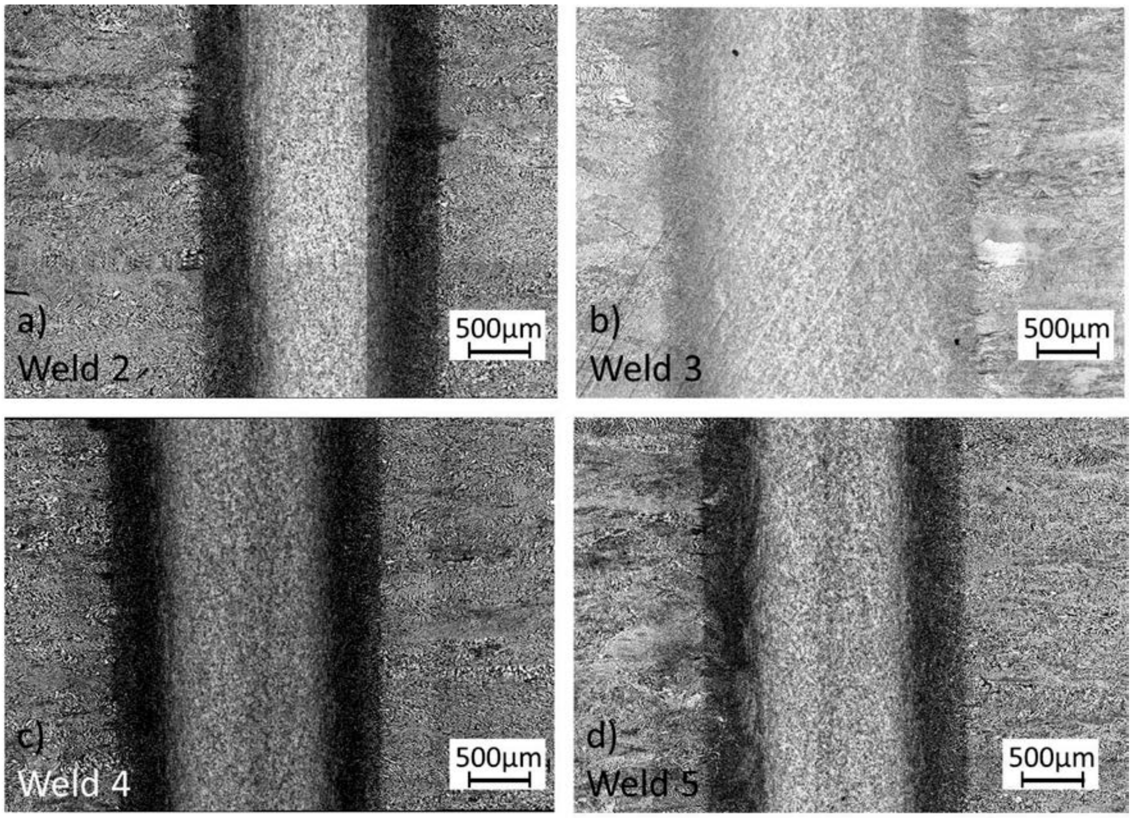

Figure 4: *Optical microscopy illustrating the parent, HAZ and TMAZ zones measured from a) weld 2, b) weld 3, c) weld 4, d) weld 5.*

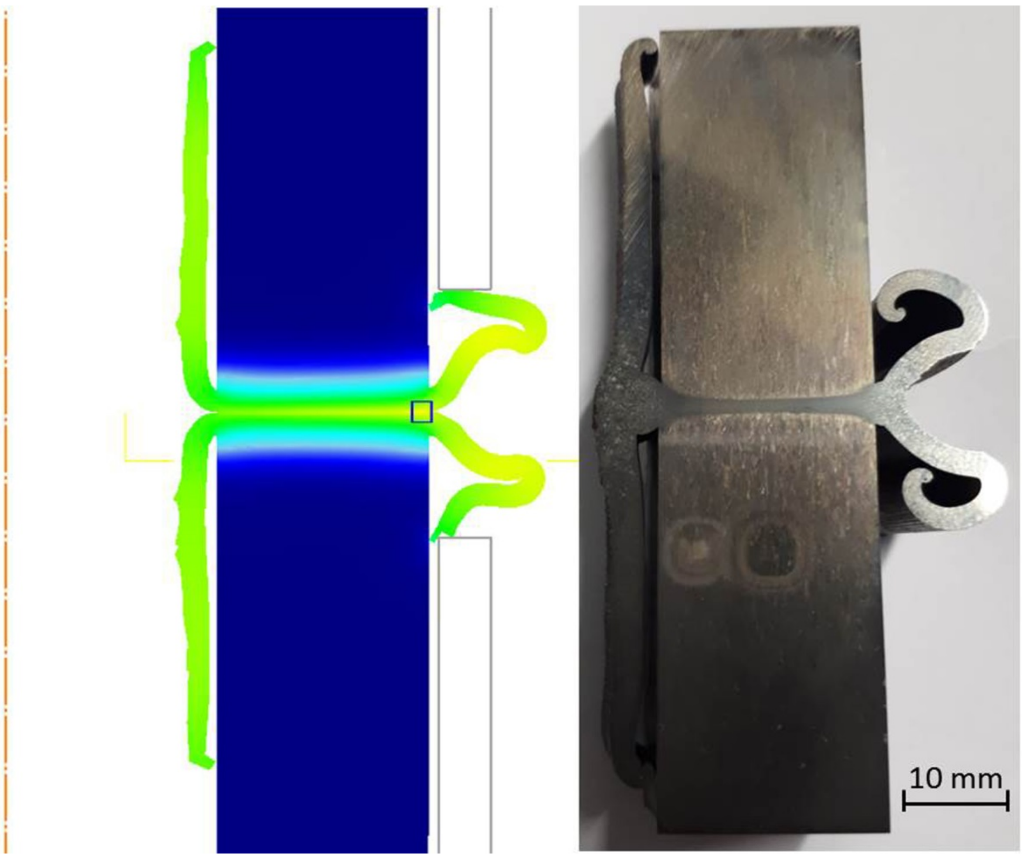

Figure 5: *Comparison of macro-scale flash appearance within the model and the real process.*

HAZ predictions

HAZ width FE predictions for the five welds were critically compared with their experimental counterparts. An example of the thermal profile generated by FE modelling for one of the welds is presented in Figure 6. For the higher energy, higher pressure welds 1 and 2 the FE model predicted the HAZ width (based upon thermal fields alone) with reasonable accuracy, within approximately 15% of the measured HAZ width, shown in Table 2. However, the HAZ width in low pressure welds was not captured as well by the "thermal field"-only prediction. Whilst the model for weld 3 substantially over-predicted the HAZ width, the models for welds 4 and 5 substantially under-predicted.

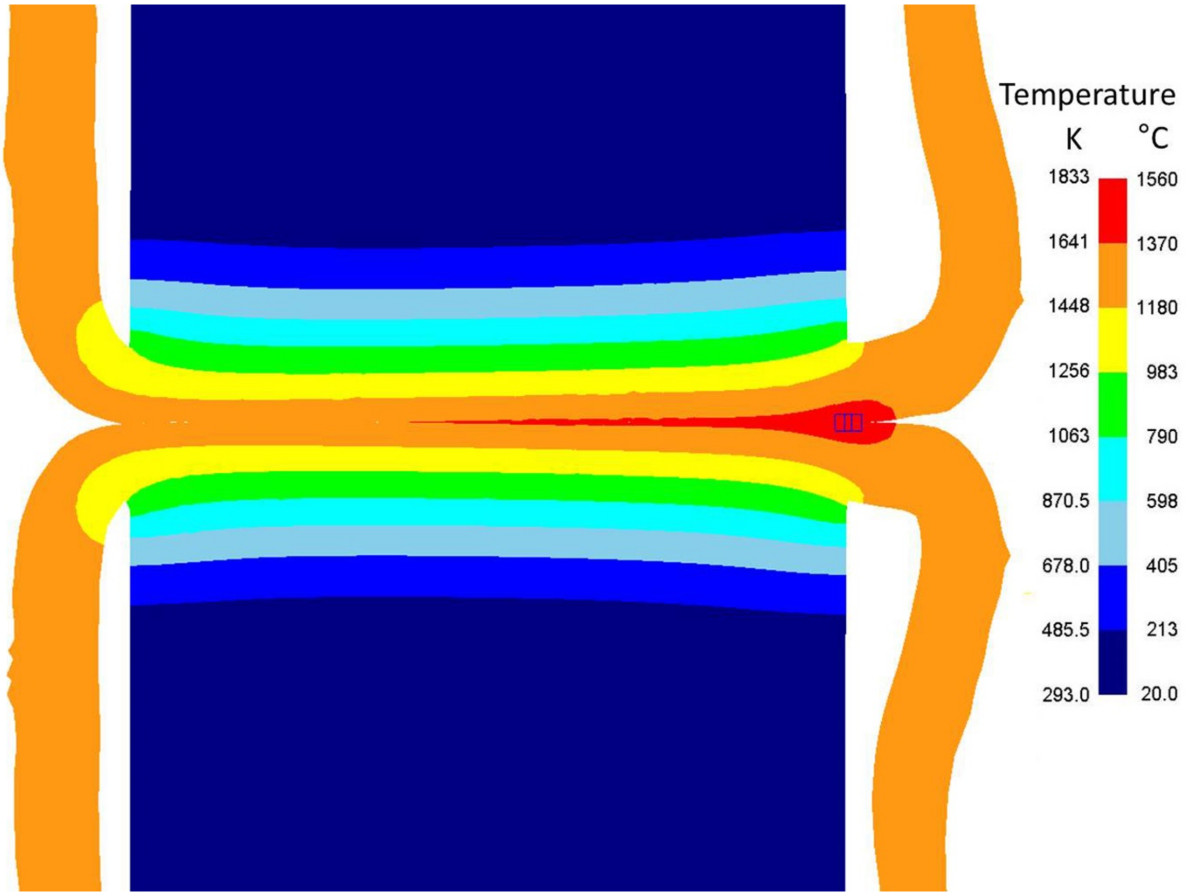

Figure 6: *FE Predicted thermal profile for a weld model. The scale indicates temperatures from RT up to 1833 K (1560 °C). Note that the green-to-yellow boundary indicates the β-transus temperature*

Table 2: *Heat-affected Zone results from FE model and weld experiment sectioning*

Weld No.	FE predicted peak weld line temperature K (°C)	FE predicted HAZ width (per "band") (mm)	Experimentally measured HAZ width (mm)	Rotational speed at max HAZ width (rad/s)	% of energy used in flywheel at max. HAZ width
1	1708 (1435)	2.4	2.05	65.5	87%
2	1688 (1415)	2.7	2.22	76	83%
3	1481 (1208)	1.8	2.51	43.5	79%
4	1408 (1135)	1.4	2.49	33.5	90%
5	1383 (1110)	1.0	2.32	30.25	93%

The effect that the individual parameters has on HAZ width, and thermal profile in general, is relatively minor for the welding process parameters considered in this work. Figure 7a shows the thermal profile for Weld 1 and 2, thus identifying that the influence that an 80MPa to 100MPa pressure has upon the profile is minor. Figure 7b shows a more substantial variation in thermal profile for a similar percentage change in the initial rotational speed. This is rationalized by the fact that the total energy available for the process varies with the rotational speed squared.

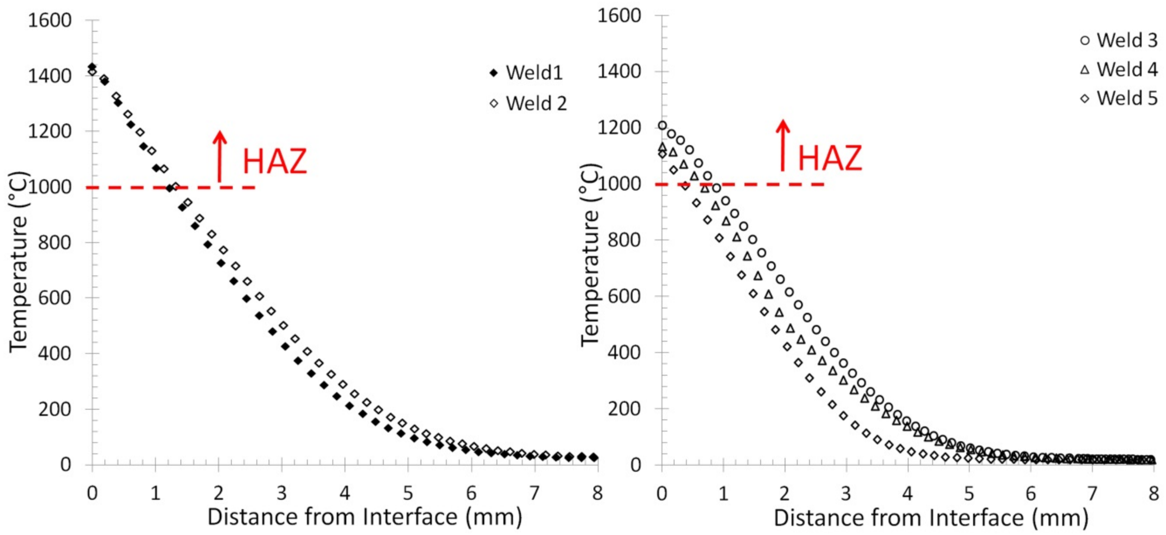

Figure 7: Predicted thermal profiles for one half of the weld, at steady-state section of welding time, for FE models varying; a) the applied pressure and b) the initial rotational speed during the IFW process

The maximum width of the band of material which has been transformed above the β-transus temperature was predicted to occur before the completion of the rotational motion, for every weld. Although difficult to experimentally corroborate these findings, this hypothesis can be rationalized due to the constantly decreasing rate of rotational motion in an Inertia weld process. At some instant, it can be rationalized that the rate of heat energy being inputted through frictional effects at the interface must fall below the rate at which heat energy is being dissipated via conduction, convection and radiation.

The rotational speed of the rotating workpiece, at the instant that maximum width of β-transus exceeding material was noted for each of the models is given in Table 2. Also given is the percentage of the available energy used to reach maximum HAZ width. For the higher energy, high pressure welds 1 and 2, an estimated 87% and 83% of the available energy respectively was dissipated in to the weld at the time the maximum HAZ band was predicted. As the applied pressure is increased, so the maximum HAZ width is predicted to occur closer to the end of the inertia weld process. Thus the results suggest a very small sensitivity of the time through the Inertia weld process that the HAZ is fully formed to the applied pressure.

For the lower energy, low pressure (40MPa) welds 3 to 5, the maximum width of the HAZ band of material is predicted to occur at a similar stage through the welding process. For the lowest energy weld 3, this is predicted to occur after 79% of energy is dissipated, 89% for weld 4 and 93% for weld 5. Clearly the model is predicting a much more sensitive response of time through Inertia welding to fully form the HAZ to the initial rotational speed, compared to the sensitivity to the pressure, primarily because the total energy is calculated using this initial rotation speed.

TMAZ predictions

The FE model was interrogated for the plastic strain field at the localized bond line region. A simplistic approach was adopted whereby the Von Mises plastic strain fields were plotted perpendicular to the weld interface. Figure 8 illustrates an example of a plastic strain field FE prediction over the workpiece. The Von Mises formulation of plastic strain was selected as this was considered the best modelling output to reflect the true effective strain observed by different locations within the three-dimensional component across the three principal axes of the polar co-ordinate geometry, namely the radial (r), vertical (z) and rotational (θ) axes.

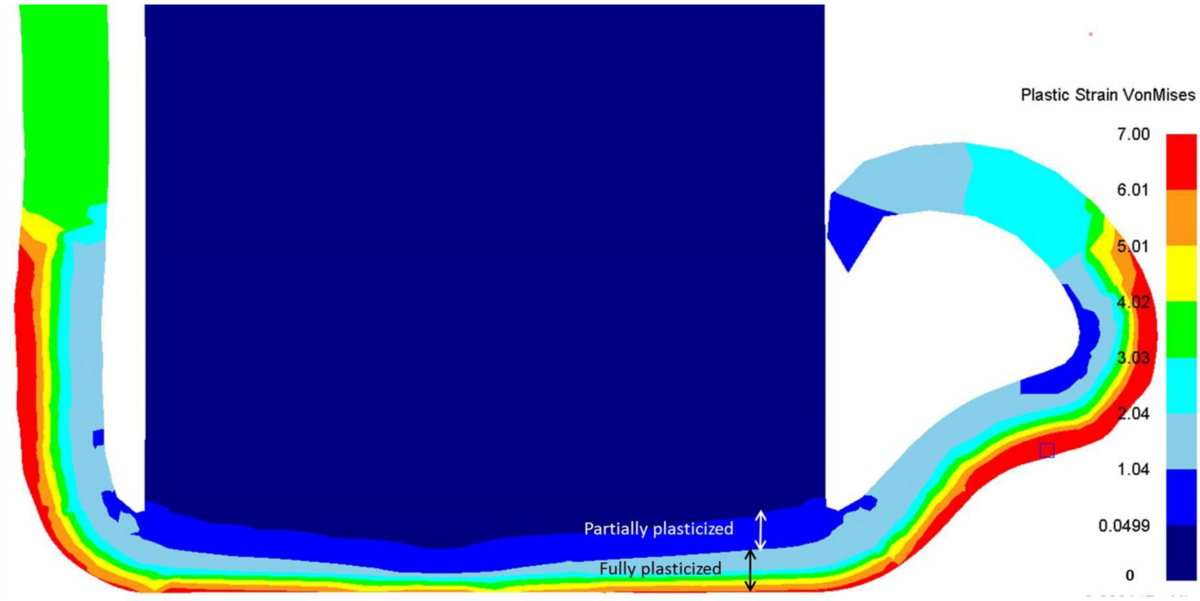

Figure 8: *FE predicted Von Mises plastic strain field for an IFW weld model.*

The FE prediction has been interrogated to attempt to quantify the fully and partially plasticized zones of an inertia weld, as described by Maalekian [5]. Although the magnitude of plastic strain within the fully and partially plasticized regions is somewhat sensitive to the process parameters, an approximation based upon the FE predictions would suggest that a Von Mises plastic strain of between 0.05 – 1.0 would describe the partially plasticized band of material, whereas a Von Mises plastic strain above approximately 1.0 indicates a fully plasticized band of material.

Table 3: *Thermo-mechanically affected zone results from FE model and weld experiment sectioning*

		TMAZ width	
Weld No.	FE predicted peak weld line plastic strain (-)	FE predicted (mm)	Experimental measured (mm)
1	5.9	1.25	1.202
2	5.6	1.35	1.091
3	0.9	1.5	1.547
4	0.52	1.0	1.306
5	0.28	0.6	1.347

As the Von Mises plastic strain predicted perpendicular to the weld line has an uncertainty associated with it, it was decided to truncate the plastic strain and consider it to have fallen back to the parent material property when the Von Mises plastic strain value fell below an absolute plastic strain value of 0.05, whichever were greater. Thus, predicted TMAZ trends shown in Table 3 are quoted as the plastic strain region which exceeds 0.05. For welds 1 and 2, the trend displayed by the FE model with this relatively simplistic approach suggests reasonable agreement with experiment. Figure 9a shows minimal plastic strain variation over the majority of the interface for an 80MPa and a 100MPa weld, although in the closest 0.5mm either side of the weld line there is noticeably a higher plastic strain for the higher applied pressure.

For welds 3-5, which varied the initial rotational speed, the FE model plastic strain field alone upon analysis gives a reasonable TMAZ width prediction for the 115 rad/s weld 3, although the model rapidly quickly becomes worse at predicting the TMAZ width as the initial speed decreases. Weld 5, with 96 rad/s initial speed, when critically compared to experiment only predicts the TMAZ width with an estimated accuracy of 50%. The effect of the varying initial rotational speed on the plastic strain field is considered for FE model predictions in Figure 9b. This again shows substantial variations in plastic strain distribution over a 2.5mm band either side of the weld line. This is likely due to the fact that available energy scales with the rotation speed, ω^2, and the total energy has to be the driving force behind plastic deformation.

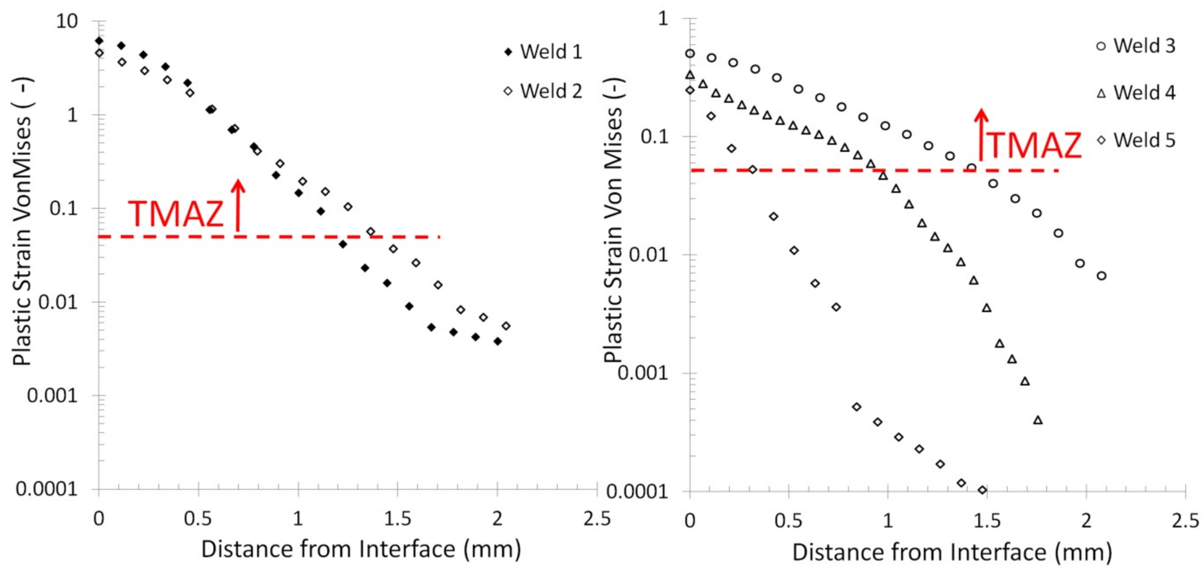

Figure 9: Predicted Von Mises plastic strain profiles for one half of the weld, at steady-state during welding time, for various FE models; a) varying the applied pressure and b) varying the initial rotational velocity during the IFW process.

Notably the FE model consistently under-predicted the TMAZ width for the low-energy welds 3-5. These welds observe minimal flash formation experimentally, and the flash formed may largely be due to asperity removal rather than steady-state burn-off. Hence it becomes clear from the formulation of an FE model, with perfectly flat faying surfaces, why such a model might struggle to capture the intricacy of the process for low-energy welds where the experimentally observed deformation and plastic strain is small and not necessarily formed by the process mechanism that the model is tailored to simulate.

The predictions of HAZ and TMAZ for welds based upon FE predicted thermal and plastic strain fields alone appear reasonable, assuming the weld isn’t very low energy. However, it is well understood that the metallurgical phenomena dictating the HAZ and TMAZ regions are far more complex than this simplistic snap-shot, and depend not only on peak temperatures or plastic strains but upon heating and cooling rates, shear zones, dislocation densities and dislocation pile-up, which in turn dictate the grain size and grain boundaries. However, the simplicity of a purely thermal-only or purely plastic strain-only field in the case of an inertia weld, particularly for the small sample size used in these welds and models with an outer diameter of 80mm and a wall-thickness of 20mm, is hypothesized to be able to reasonably predict the HAZ and TMAZ zones due to the speed at which the process occurs. With the welding process occurring within typically 3-4 seconds, and the subsequent air cooling meaning that the weld region falls to well below the β-transus temperature within this short 4-second process window, the rapidity of an inertia friction weld actually restrict the metallurgical process phenomena given that they are ‘time-at-temperature’ dependent.

Impact of processing conditions on phase transformation

Within an IFW process the time that the material is held at elevated temperature is very short. The processing conditions, including the pressure and experienced heating and subsequent cooling rates have a significant impact upon the solid-state phase transformation of the hexagonally-close packed α phase structure transforming to the body-centered cubic β phase structure in titanium alloys [27].

The effect of pressure on the solid state phase transformation can be estimated using the Clausius-Clapeyron relation, namely:

$$\frac{dP}{dT} = \frac{L}{T\Delta v} \qquad \text{Equation 2}$$

whereby P is the Applied pressure, T the temperature, L the latent heat and Δv the specific volumetric change. The specific volumetric change associated with the phase transformation is accordingly the difference between the specific volumes of α phase and β phase, approximately 5.5 x 10^{-6} m^3. This allows for a calculated change in temperature of the β-transus, for a pressure of 100MPa, and a latent heat of Ti-6Al-4V of 678 x 10^3 Jkg^{-1} [28], and an assumed initial β-transus temperature of 1256 K (983°C), resulting in ΔT = 1.65 K. Thus, the Clausius-Clapeyron relation has demonstrated that for the pressure considered by the processing, the shift in β-transus temperature is negligible.

Whereas, the effect of cooling rate upon the effective β-transus is understood to be much greater. It is hypothesized that there will be locations inside the HAZ of the IFW sample, which have exceed the β-transus temperature but for an insufficient time for the transformed β phase structure to form. Therefore the microstructure within the TMAZ and the HAZ requires further analysis at a smaller length scale than can be achieved with optical microscopy.

Figure 10 illustrates SEM images of the microstructure observed at five specific locations within weld 1, namely at locations; a) within the parent material, b and c) at different locations within the region that has been heated to exceed the β-transus but held for a short period such that the phase transformation is only partially undergone (HAZ-like features), d) inside the HAZ, and e) inside the TMAZ. The parent microstructure at location (a) illustrates the familiar globular α phase and a fine lath structure of interlayered α and β laths. The image shown in (b) is from a location that has exceeded the β-transus for the Ti-6al-4V alloy, however the heating and cooling process has occurred so fast, and the material exceeded the β-transus temperature for a fraction of a second. Thus the phase transformation has not fully occurred. The image displays the “ghost” microstructure that is observed in rapid heating and cooling rate processes. Therefore the α phase is has not been able to fully transform, and the needle-like structure of an α-β alloy is observed, although with retained α phase present as a dissolute phase.

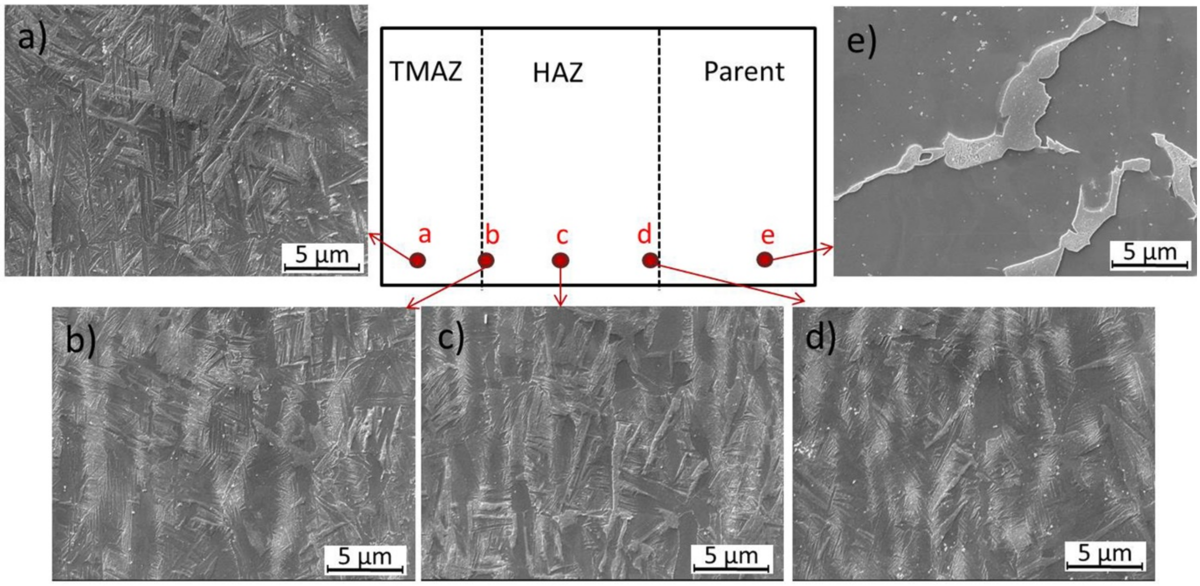

Figure 10: SEM analysis of weld 1 at locations a) within parent material, b) & c) within material that exceeds β-transus for a short time such that the transformation is incomplete, d) within the HAZ and e) within the TMAZ.

Location (c) illustrates the material at another location which has exceeded the β-transus temperature for the alloy, and for a little longer than location (b), but still not enough to allow the full allotropic transformation. The same "ghost" microstructure as (b) is observed with the dissolute retained α phase, except here there is evidence of the β phase beginning to recrystallize as well. Thus it becomes apparent that during the allotropic phase transformation, the dissolution of the α phase is the first crystallographic feature to change, followed by the β-phase recrystallization.

Location (d) illustrates a more typical heated Ti-6Al-4V microstructure, forming the familiar lath structure of α phase interweaved with the β phase, enriched with the β-phase stabilizing vanadium. This structure is referred to commonly as hexagonal α'-type titanium martensite [27]. Comparing location (d) to locations (c) and (b) highlights the impact on the allotropic transformation that heating and cooling rates can have, and thus illustrates the not-insignificant shift towards hotter temperatures in the "effective" or "observed" β-transus.

Location (e) considers material that has been held at temperature above the β-transus for long enough for the phase transformation to fully occur, plus it has additionally undergone a mechanically-induced deformation caused by the shearing motion at the interface. Therefore these regions can be identified by the alignment of the grains with the interface, as during the IFW process the grains have been sheared by the interfacial frictional forces.

Finally, when performing a microstructural analysis within the HAZ and TMAZ regions of an inertia weld, one must consider the physical conditions of the sample during the processing route, and the impact that these conditions have upon the microstructure observed within the specimen. The flow stresses of the mixed phase solid and liquid states [29] and of separate α and β-phases [30] of the titanium alloy have been studied and experimentally tested for their flow characteristics and behavior. It is reported [30] that the β-phase material, at temperatures just below the β-transus for the alloy Ti-6Al-4V, is considerably softer than the α-phase material. Work by Mulyadi *et al* [30] suggests a flow stress at a rate of $0.3s^{-1}$ of approximately 60MPa for the soft β-phase, and 160MPa for the α-phase. Whilst the measurements suggest that the α-phase is softening more rapidly with increasing temperature than the β-phase, it is probable that even at higher temperatures including the weld line temperatures in an inertia weld, the β-phase remains substantially easier to deform under load. For the inertia welds in this work with high applied pressure, the softer β material is likely to be easily ejected out of the weld zone and in to the flash material - simply by the higher applied load compressing the heated material. Thus, the microstructure remaining within the weld line and at locations close to edge of the inertia weld specimen may not be representative of the microstructure of the heated material at the central regions of the inertia weld, as it is likely to be depleted of the softer, easier to extrude β-phase. Additionally, this region of material where β-phase has likely been ejected faster than the α-phase may display different strain and shearing bands because this softer β-phase material is able to escape the compressive loading of the weld through ejection in to the flash. These two-phase microstructural complexities have not been included within the current modelling framework.

Conclusions

A fully coupled thermo-mechanical finite element modelling strategy was developed to predict the thermal and mechanical loading occurring close to the interface region of a titanium alloy inertia friction weld joint. In order to validate the FE model, experimental measurements of the HAZ and the TMAZ were made. The following conclusions can be drawn:

- The FE model predicts the width of the HAZ material using this simplistic thermal-only consideration with an error of approximately 15%, for welds 1 and 2, with higher total energy input. However, for welds 3-5 with lower total energies, the error of prediction exceeds 50% in worst cases. Errors are likely due to small metallurgical influences that a thermal-only prediction neglects to consider.
- The FE model predicts the width of the TMAZ material using this simplistic plastic strain-only consideration with an average error of approximately 13%, for welds 1 and 2, Welds 3 and 4 also have reasonable errors of 15% or smaller, but weld 5 – the lowest energy weld, again has a considerable error. Errors are likely due to small metallurgical influences that a strain-only prediction neglects to consider.
- The plastic strain FE predicted field has been used to hypothesize that the fully-plasticized material described by Maalekian in the literature has a plastic strain component exceeding 1.0, whereas the partially plasticized material has a plastic strain of between 0.05 and 1.0.
- The solid-state transformation temperature within Inertia welds is impacted only minimally by the pressures considered within the process, but evidence suggests it is impacted significantly by the heating and cooling rates experienced.

Acknowledgements

Parts of this work were carried out as a part of the Centre for Advanced Simulation and Modelling for Manufacture (CASiM^2) project. The authors wish to acknowledge the project partners Rolls-Royce plc and the MTC, as well as funding body the ERDF for supporting this work. Thanks are offered to Dan Howe, Ben Saunders and Dr Simon Bray (all at Rolls-Royce plc), Dr Hannah Edmonds and Dr Pedro

Santos (both MTC) and Dr Joao Gandra (TWI) for expert advice and help with the experimental inertia friction weld trials. Thanks to Wilde Analysis for providing Deform v11.0.2 software technical support. Material models were constructed with assistance from Sente Software's JMatPro database.

References

1. A. Chamanfar, M. Jahazi, J. Cormier, *Met Trans A*, 2015, 46A, pp1639-1661.
2. M.B. Uday, M.N. Ahmad-Fauzi, A.B. Ismail, *Science and Technology of welding and joining*, 2010, 15;7 pp534-558.
3. D. Baffari, G. Buffa, D. Campanella, L. Fratini, F. Micari, *Procedia CIRP,* 2014, 18; pp162-167.
4. R.P. Turner, J-C. Gebelin, R.M. Ward, R.C. Reed, *Acta Mater*., 2011, 59;10, pp3792-3803.
5. M. Maalekian, *Science and Technology of welding and joining*, 2007, 12;8, pp738-759.
6. H. Kreye, *Welding Research Supplement*, 1977, May'77,pp154-158.
7. M. Preuss, P.J. Withers, J.W. Pang, G.J. Baxter , *Met Trans A,* 2002, 33;10 , pp3215-3225.
8. M. Preuss, P.J. Withers, J.W. Pang, G.J. Baxter, *Met Trans A*, 2002, 33;10, pp3227-3234.
9. C.G. Nessler, D.A. Rutz, R.D. Eng, P. Vozzella, *Welding Research – supplement to the Welding Journal*, 1971, September '71.
10. M.M. Attallah and M. Preuss, Welding and Joining of Aerospace Materials (Chapter 2), 2012, Woodhead Publishing.
11. C.L. English, Fabtech International '95, 1995, Chicago, USA.
12. W.A. Baeslack III, D. Phillips, C. English, A.P. Woodfield, *Journal of Materials Science Letters,* 1991, 10, pp 1401–1408.
13. A. Barussaud and A. Prieur, Titanium '95 – Science and technology; the 8th World Conference on Titanium, 1995. Birmingham, United Kingdom.
14. Y. Pardhi, C. Dungey, G. Baxter, P. Bowen, T.P. Halford, *Journal of ASTM International*, 2010, 7:6, pp 14.
15. A. Yates, M.Res thesis, 2015, University of Birmingham, UK.
16. C. Bennett, *J. Manuf. Proc*., 2015, 18; pp84-91.
17. Manufacturing Technology, Inc., 1702 West Washington, South Bend, IN, 46628 USA.
18. G. Van de r Voort*, Buehler Tech Notes*, 2015, 3:3 , https://buehler.com/China/solutions/technotes/vol3_issue3.pdf
19. B. Grant, M. Preuss, P.J. Withers, G. Baxter, M. Rowlson, *Mat. Sci. Eng. A,* 2009, 513-4; C, pp366-375.
20. L. D'Alvise, E. Massoni, S.J. Walloe, *J. Mat. Proc. Tech*, 2002,125-126, pp387-391
21. C.J. Bennett, M.M. Attallah, M. Preuss, P.H. Shipway, T.H. Hyde, S. Bray. *Met Trans A.* 2013, 44;11, pp5054-5064.
22. R.P. Turner, D. Howe, B. Thota, R.M. Ward, H.C. Basoalto, J.W. Brooks, *J. Manuf. Proc*., 2016, 24:1, pp186-94
23. R.P. Turner, D. Howe, B. Thota, R.M. Ward, H.C. Basoalto, J.W. Brooks, OPTIMoM Conference, 2014, Oxford, UK.
24. W. Li, S. Shi, F. Wang, Z. Zhang, T. Ma, J. Li, *JESTR*, 2012, 5;3, pp10-19.
25. N. Saunders, Z. Guo, X. Li, A.P. Miodownik and J.P. Schillé, *Journal of Metals*, 2003, 55;12, pp60 .
26. Deform Training, Scientific Forming Technologies Corporation, 2545 Farmers Drive, Suite 2000, Columbus, OH.
27. I.J. Polmear: The Light Alloys, 2005, Butterworth-Heinemann.
28. M. Villa, PhD thesis, 2015,University of Birmingham, UK.
29. M. Boivineau, C. Cagran, D. Doytier, V. Eyraud, M-H. Nadal, B. Wilthan and G. Pottlacher, *Int. J. Thermopyhsics*, 2006,27:2 pp507-529.
30. M. Mulyadi, PhD thesis, 2007, Open University, UK.

List of Figure Captions

Figure 1: Schematic of an inertia weld on a hollow cylinder, showing a macro-scale representation of the banding of parent, HAZ and TMAZ material.

Figure 2: Elongated α grain in a transformed β matrix at x50 magnification

Figure 3: An example of the FE modelling set-up for the IFW modelling in Deform v11.0.

Figure 4: Optical microscopy illustrating the parent, HAZ and TMAZ zones measured from a) weld 2, b) weld 3, c) weld 4, d) weld 5.

Figure 5: Comparison of macro-scale flash appearance within the model and the real process.

Figure 6: FE Predicted thermal profile for a weld model. The scale indicates temperatures from RT up to 1833 K (1560 °C). Note that the green-to-yellow boundary indicates the β-transus temperature

Figure 7: Predicted thermal profiles for one half of the weld, at steady-state section of welding time, for FE models varying; a) the applied pressure and b) the initial rotational speed during the IFW process

Figure 8: FE predicted Von Mises plastic strain field for an IFW weld model.

Figure 9: Predicted Von Mises plastic strain profiles for one half of the weld, at steady-state section of welding time, for FE models; a) varying the applied pressure and b) varying the initial rotational velocity during the IFW process.

Figure 10: SEM analysis of weld 1 at locations a) within parent material, b) & c) within material that exceeds β-transus for a short time such that the transformation is incomplete, d) within the HAZ and e) within the TMAZ.

List of Table captions

Table 1: Process parameters used in IFW FE modelling and experimental trials.

Table 2: Heat-affected Zone results from FE model and weld experiment sectioning

Table 3: Thermo-mechanically affected zone results from FE model and weld experiment sectioning

Table 1: Process parameters used in IFW FE modelling and experimental trials.

Weld No.	Inertia value (kgm^2)	Initial rotation speed (rad/s)	Pressure (MPa)	Total Energy ½$I\omega^2$ (kJ)	Resulting Experimental Upset (mm)
1	18.6	185	100	637	14.1
2	18.6	185	80	637	13.1
3	18.6	115	40	246	2.3
4	18.6	105	40	205	1.6
5	18.6	96	40	171	1.1

Table 2: Heat-affected Zone results from FE model and weld experiment sectioning

Weld No.	FE predicted peak weld line temperature K (°C)	FE predicted HAZ width (per "band") (mm)	Experimentally measured HAZ width (mm)	Rotational speed at max HAZ width (rad/s)	% of energy used in flywheel at max. HAZ width
1	1708 (1435)	2.4	2.05	65.5	87%
2	1688 (1415)	2.7	2.22	76	83%
3	1481 (1208)	1.8	2.51	43.5	79%
4	1408 (1135)	1.4	2.49	33.5	90%
5	1383 (1110)	1.0	2.32	30.25	93%

Table 3: Thermo-mechanically affected zone results from FE model and weld experiment sectioning

		TMAZ width	
Weld No.	FE predicted peak weld line plastic strain (-)	FE predicted (mm)	Experimental measured (mm)
1	5.9	1.35	1.202
2	5.6	1.35	1.091
3	0.9	1.5	1.547
4	0.52	1.0	1.306
5	0.28	0.6	1.347